Theor Chem Acc (1999) 101:97–102
DOI 10.1007/s002149800m74

Theoretical
Chemistry Accounts

Regular article

Ion channels of biological membranes: prediction of single channel conductance*

Kishani M. Ranatunga[1], Charlotte Adcock[1], Ian D. Kerr[2], Graham R. Smith[1], Mark S. P. Sansom[1]

[1] Laboratory of Molecular Biophysics, University of Oxford, Rex Richards Building, South Parks Road, Oxford, OX1 3QU, UK
[2] Nuffield Department of Clinical Biochemistry, University of Oxford, Institute of Molecular Medicine, John Radcliffe Hospital, Oxford, OX3 9DS, UK

Received: 25 May 1998 / Accepted: 4 August 1998 / Published online: 2 November 1998

Abstract. The Poisson-Boltzmann equation was solved numerically for models of the pore regions of the *Shaker* K^+ channel and of two glycoporins (LamB and ScrY) to yield electrostatic potential profiles along the pore axes. From these potential profiles, single-channel current-voltage (*I–V*) relations were calculated. The importance of a proper treatment of the ionisation state of two rings of aspartate sidechains at the mouth of the K^+ channel pore emerged from such calculations. The calculated most likely state, in which only two of the eight aspartate sidechains were deprotonated, yielded better agreement with experimental conductance data. An approximate calculation of single-channel conductances based simply on pore geometry yielded very similar conductance values for the two glycoporins. This differed from an experimentally determined conductance ratio of ScrY:LamB = 10:1. Preliminary electrostatics calculations appeared to reproduce the observed difference in conductance between the two glycoporins, confirming that single-channel conductance is determined by electrostatic as well as geometric considerations.

Key words: K^+ channel – Glycoporin – LamB – ScrY – Conductance

1 Introduction

Channels are integral membrane proteins which permit the passive movement of selected inorganic ions across lipid bilayer membranes [1]. They are central to the electrical activity of excitable cells (e.g. neurons, muscle), but are also found in membranes of a wide range of organisms and cells, from viruses to plants. Patch clamp recording techniques [2] allow ionic currents flowing through single-channel molecules to be measured as a function of the voltage across the membrane, thus yielding current-voltage (*I–V*) relationships, from which single-channel conductances may be derived. In principle it should be possible to calculate such *I–V* relationships from structural models of channels. However, this process is impeded by our lack of knowledge of three-dimensional structures for ion channels (although the recent publication of an X-ray structure for a bacterial K^+ channel [3] indicates that this may improve in the near future) and by our imperfect understanding of the theory relating ion channel structure to function [4]. In particular, it remains to be established what is the appropriate level of detail at which to describe ion permeation in order to obtain an accurate prediction of a single channel conductance. One approach, suggested by Hille [1] and explored in more detail by Smart et al. [5], stresses the importance of channel geometry, as embodied in the pore radius profile of a channel, in determining single-channel conductance. However, such an approach masks the possible importance of electrostatic interactions between channel and permeating ion. In particular, an ion passing through a channel of molecular dimensions is likely to interact strongly with ionised sidechains lining the channel. ''Rings'' of such sidechains have been suggested to play an important role in ion permeation and selectivity of, for example, the nicotinic acetylcholine receptor [6]. However, as noted by a number of authors [6–8], one may not assume that ionisable sidechains within a channel environment will adopt their ''normal'' bulk solution ionisation state. Thus, even an approximate theory of ion permeation must take into account pore geometry, the presence of ionisable sidechains within and at the mouths of the pore, and the ionisation state of such sidechains. In this paper we explore such considerations for two types of channel: (1) a model of the pore domain of the *Shaker* voltage-gated K^+ channel; and (2) the glycoporins LamB (maltoporin) and ScrY (sucrose porin), for which high-resolution X-ray structures are available [9, 10].

*Contribution to the Proceedings of Computational Chemistry and the Living World, April 20–24, 1998, Chambery, France

Correspondence to: M.S.P. Sansom
e-mail: mark@biop.ox.ac.uk, Tel.: +44-1865-275182,
Fax: +44-1865-275182

2 Methods

The program HOLE [11] was used to characterise the geometry of the structures, yielding a profile of the radius along the pore axis. This may then be used to give a first approximation to the channel's Ohmic conductance by assuming that the resistance of the channel may be obtained from the sum of the resistances of a series of cylinders with the same resistivity (ρ) as that of bulk electrolyte in solution:

$$G_{\text{upper}}^{-1} = \sum_{z=\text{low}}^{z=\text{high}} \frac{\rho \Delta L}{\pi r_z^2}, \tag{1}$$

where G_{upper} is the upper limit to the channel conductance, r_z is the radius of each cylinder, ΔL is its length, and where z lies along the length of the pore. The resulting value embodies the assumptions that conductance can be determined purely by channel geometry and that water and ions within the channel have bulk-like behaviour. To correct for the difference between the resistivity of an electrolyte in its bulk state and within a channel, we employ the approximation described in [5]:

$$G_{\text{pred}} = S \cdot G_{\text{upper}} \tag{2}$$

where G_{pred} is the predicted conductance and $S = 0.2$ is an empirical scale factor based on fitting to known channel structures and conductances.

It is also possible to calculate a channel's conductance by a more detailed consideration of its electrostatic characteristics. We use the program UHBD [12] to calculate values for the electrostatic potential by solving the linear Poisson-Boltzmann equation using a finite-difference method:

$$\nabla \cdot (\varepsilon(\mathbf{r}) \nabla \phi(\mathbf{r})) - \kappa^{-2}(\mathbf{r}) \phi(\mathbf{r}) + 4\pi\rho(\mathbf{r}) = 0 \tag{3}$$

where ϕ is the electrostatic potential, ε is the dielectric constant, and κ is the modified Debye-Huckel parameter. The protein is embedded in a low dielectric ($\varepsilon = 4$) slab and the solvent, both inside and outside of the pore, is modelled with a dielectric of 78. On the basis of such calculations one may determine the following characteristics of the channel: (1) the ionisation states of titratable groups; (2) the electrostatic profile along the pore axis; and (3) the single-channel I–V relationship.

The standard pK_A for an ionisable amino acid sidechain is for that sidechain when in an isolated amino acid in dilute aqueous solution. The intrinsic pK_A for the same sidechain is for when it is within a protein environment, assuming all other sidechains in the protein are in their uncharged state. The difference between the standard and intrinsic pK_A values may be obtained via calculation (using UHBD) of the solvation energies of the sidechain in the two states. By considering the interaction of a residue with all other ionisable groups in the protein in all their possible ionisation states, a titration curve for that residue may be calculated from which the absolute pK_A may be obtained. Using the absolute pK_A, the ionisation state of that residue at physiological pH (i.e. 7) may be obtained. A more detailed description of the general methodology of calculating the pK_A of an ionisable group may be found in [13] and [14].

Once the ionisation state of all residues in a pore model has been calculated, one may use the Poisson-Boltzmann equation to calculate the resultant electrostatic potential profile ϕ as a function of position along the pore (z) axis.

This electrostatic profile may be used to calculate the single-channel I–V relationship. The Nernst-Planck equation describes the flux of a charged species across a barrier to diffusion in a net transbilayer electrochemical gradient. The electrochemical gradient may be expressed as a function of the electrostatic potential to yield the Poisson-Nernst-Planck equation. Reducing the problem to one dimension (along the pore axis), the Poisson-Nernst-Planck equation becomes:

$$I_{\text{total}} = FD\beta[C]A\left(\left(-\frac{\exp(z_c F\phi_c/RT)-1}{\int_0^l [\exp(z_c F\phi_{zc}/RT)dz]}\right)+\left(\frac{\exp(z_a F\phi_a/RT)-1}{\int_0^l [\exp(z_c F\phi_{za}/RT)dz]}\right)\right), \tag{4}$$

where I is the total current, F is the Faraday constant, D is the diffusion coefficient for ion, β is the partition coefficient for ion from bulk solution to channel, $[C]$ is the salt activity (equal on both sides), A is the cross-sectional area of the channel, $z_{c/a}$ is the cation/anion valence, $\phi_{c/a}$ is the applied potential for cation/anion, $\phi_{zc/a}$ is the potential at position z in the membrane for cation/anion, and l is the effective length of the channel. This may be solved to calculate the current per unit area through the channel as a function of transbilayer potential difference, leading to a characteristic I–V relation for the channel.

3 Results

3.1 Shaker K^+ channel model

Voltage-gated potassium channels open in response to the depolarisation of the cell membrane to selectively

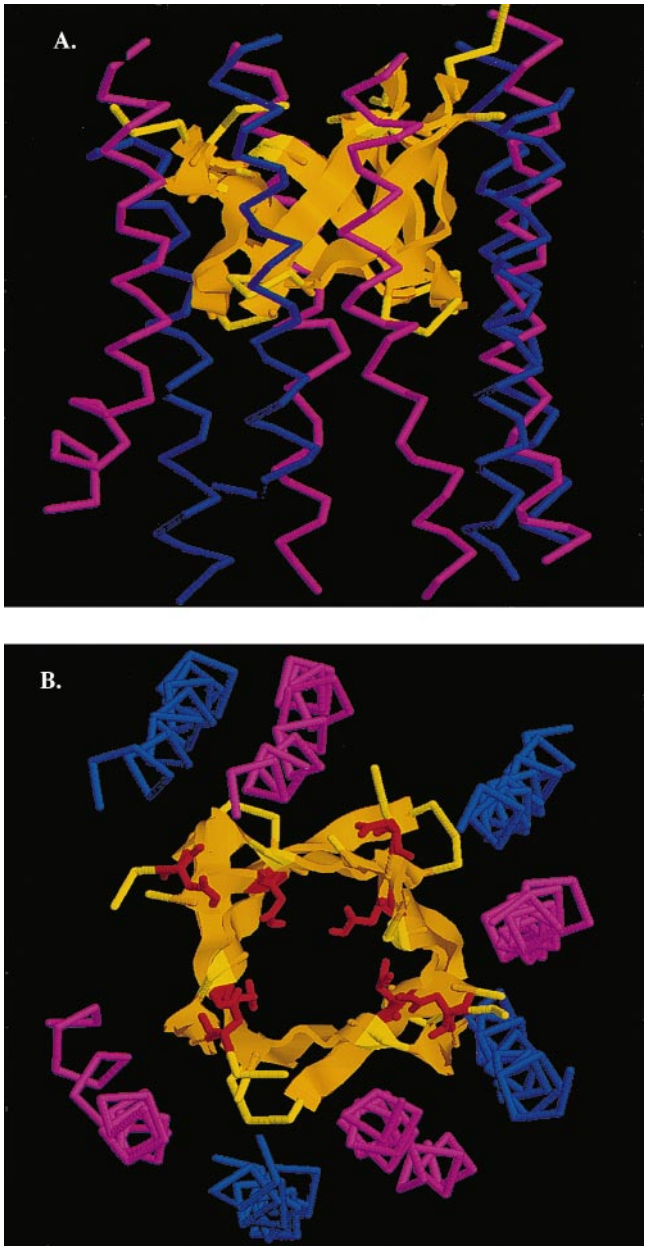

Fig. 1. **A** C-α backbone trace of *Shaker* K^+ channel pore model from side view. The H5 β-barrel is coloured orange, the S5 helices blue, and the S6 helices magenta. **B** Same model as viewed from the extracellular end of the pore. The Asp rings are represented in atomic detail and coloured red

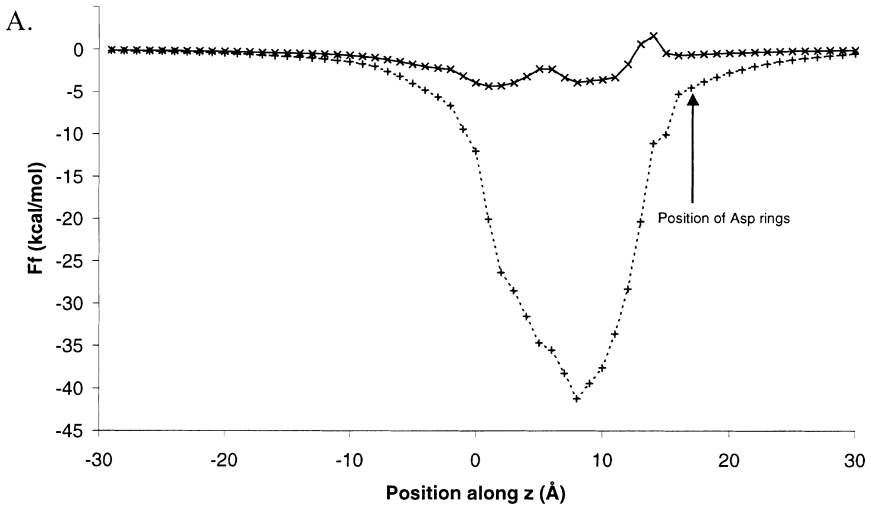

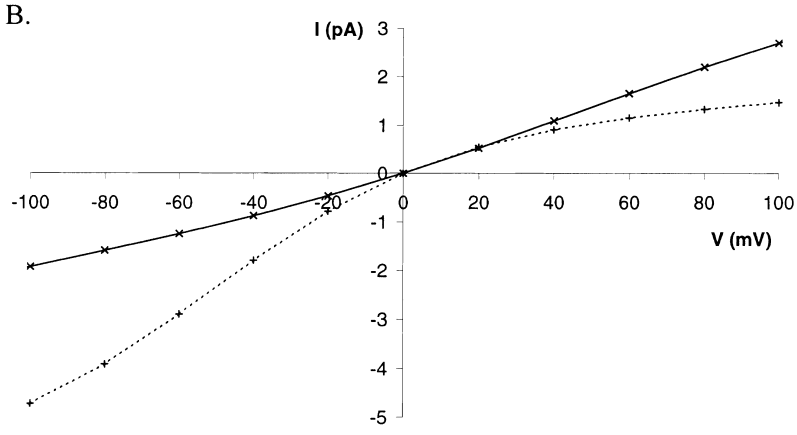

Fig. 2A,B. Results for the K^+ channel pore model. *Broken line* = all eight aspartate residues deprotonated; *solid line* = only two aspartate residues deprotonated. **A** The electrostatic potential energy for a monovalent cation passing down the pore axis is shown as a function of its position along the pore axis. **B** *I–V* relation, at an ionic concentration of 100 mM KCl

enable passive diffusion of potassium ions through them. Their physiological role is to return the membrane potential back to its resting value, thus terminating an action potential.

A model of the pore-lining region of the *Shaker* K^+ channel (see Fig. 1) was derived from a large body of mutagenesis data using a restrained molecular dynamics procedure as described previously [15]. In this model (which is not uniquely defined by the experimental data) the pore is formed by a double-bulged β-barrel (containing the P-region, or H5 loop, of the channel sequence) flanked by eight helices, S5 and S6 (see Fig. 1). A salient feature of our model is the presence of two rings of Asp residues (residues Asp2 and Asp18 from the *Shaker* sequence) near the extracellular mouth of the pore (see Fig. 1B). Also, a Tyr ring (from the GYG potassium channel sequence motif) constricts the narrowest region of the pore. Recently, an X-ray structure of a bacterial potassium channel, from *Streptomyces lividans*, has been solved to 3.2 Å [3]. Whilst our model differs from the X-ray structure in the secondary structure of the P-domain, both the model and the experimental structure would suggest that the "rings" of Asp sidechains are present at the mouth of the channel.

pK_A calculations on the two Asp rings show that, in general, only two (one from each ring) of the eight Asp sidechains are ionised. This calculation was repeated on four snapshot structures taken at 50 ps intervals through a 250 ps molecular dynamics (MD) simulation. Exactly which of the eight residues are ionised changes with respect to time, suggesting that the ionisation state may undergo dynamic transitions. It should be noted that we have not yet investigated how such transitions might change in the presence of a permeant K^+ ion.

On the basis of the pK_A calculations, electrostatic profiles (see Fig. 2A) were compared for the model with all eight Asp sidechains in their default ionisation state, with all the Asps ionised, and the most likely state in which two Asp sidechains were charged and the rest were protonated (and hence neutral). There is a marked

difference between the profiles, particularly in the region of the Asp rings at z ca. +12 to +20 Å. There is a well of a depth of just over 40 kcal/mol (i.e. $-70RT$) if one assumes all the Asp residues to be ionised. A cation within such a well would find it energetically very difficult to escape and so such a profile would not be expected to correlate with the known conductance for the channel (ca. 19 pS at 100 mM KCl [16]). With only two of the Asp residues ionised, the profile is much flatter. This difference mirrors that seen in a previous study which employed MD simulations to determine potential energy profiles for a K^+ ion moved along the pore axis of a similar channel model [8].

I–V curves (see Fig. 2B) were calculated on the basis of both of the electrostatic potential profiles. The curve for the default ionisation state is asymmetric i.e. the channel was predicted to show rectification [1]. Such rectification arises from the asymmetrical nature and large extent of the well in the electrostatic profile. In the more physically realistic case where only two of the Asps were negatively charged, the relation is linear, yielding a slope conductance of from around 20 to 25 pS. This correlates well with the experimental data [16] which indicate a linear *I–V* relationship with a single-channel conductance of 19 pS. Furthermore, for both models almost all of the current was predicted to be carried by cations, again as is the case experimentally. Thus, although clearly an approximation, and unable to describe selectivity between different cations, a simple theoretical treatment of a physically realistic model of that state of ionisation of sidechains at the mouth of a K^+ channel predicts a current-voltage relationship which is in good agreement with that obtained experimentally. This encourages one to continue to develop this theoretical approach and to apply it to other channel systems, e.g. bacterial porins.

3.2 Glycoporins

The outer membrane of Gram-negative bacteria contains two classes of porin, which facilitate the movement of hydrophilic substances across it. The general diffusion porins (five of which have X-ray crystallographically determined structures [17–20]) allow the passage of molecules and ions of less than ca. 500 Da molecular weight. Rather more specific porins are expressed under growth-limiting conditions. These contain binding sites for specific classes of solute (e.g. sugars), which are thus able diffuse at high rates for low concentrations of solute [21–23]. Two well-studied specific porins are maltoporin (also known as LamB) and sucrose porin (ScrY). Maltoporin forms a channel for the permeation of maltose and higher maltodextrins whilst sucrose porin is specific for sucrose and maltooligosaccharides. Both also form cation selective channels.

The *Escherichia coli* structures of LamB and ScrY have been determined by X-ray crystallographic techniques to 3.1 and 2.4 Å, respectively [9, 10], revealing some striking structural similarities. ScrY has a further N-terminal, non-pore 72 amino acids, but the electron density was too poor to solve this region. Each glycoporin monomer is an 18-stranded β-barrel (see Fig. 3A,B). The third external loop in each monomer folds along the inside of the barrel, constricting the pore lumen. At the constriction site there are six aromatic residues that form a "greasy slide" opposite a number of ionisable residues ("the ionic track") which serve to facilitate sugar diffusion. However, despite their overall structural similarity, the single-channel conductance of maltoporin (0.15 nS in 1 M KCl [21]) is ca. 10-fold lower than that of ScrY (1.4 nS in 1 M KCl [23]). This dif-

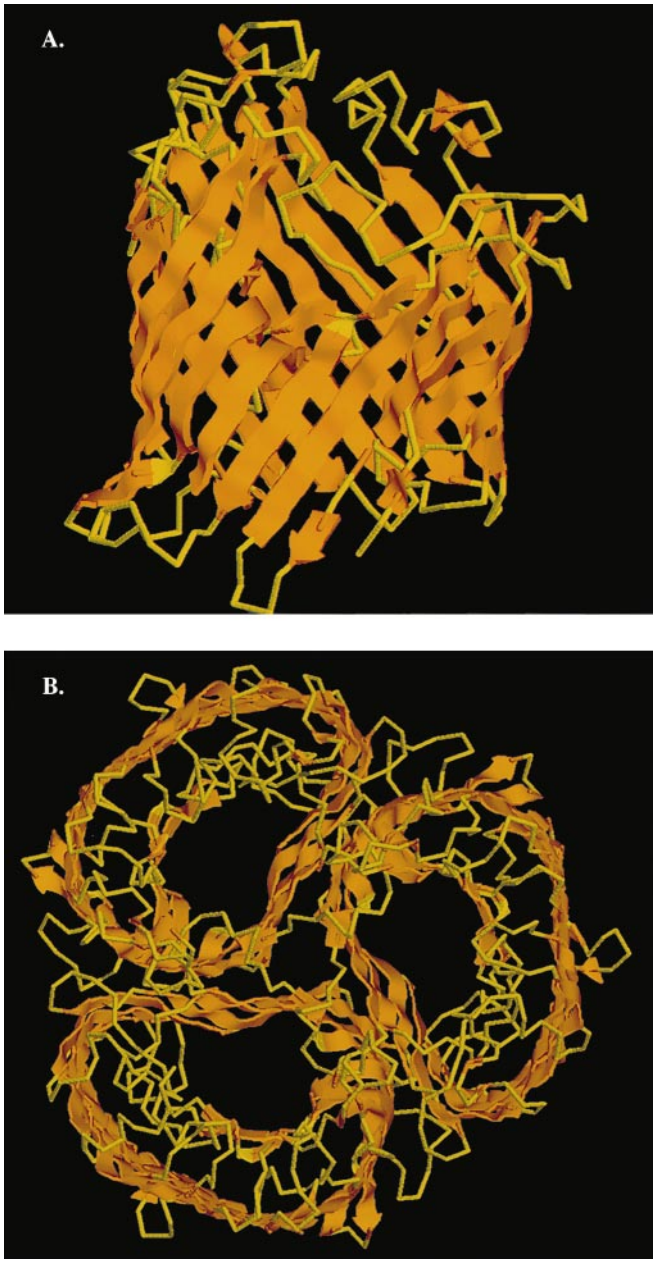

Fig. 3. **A** Side - on view of ScrY monomer. **B** View down the ScrY trimer. The β-strands are shown as orange arrows, and the interstrand loops are yellow

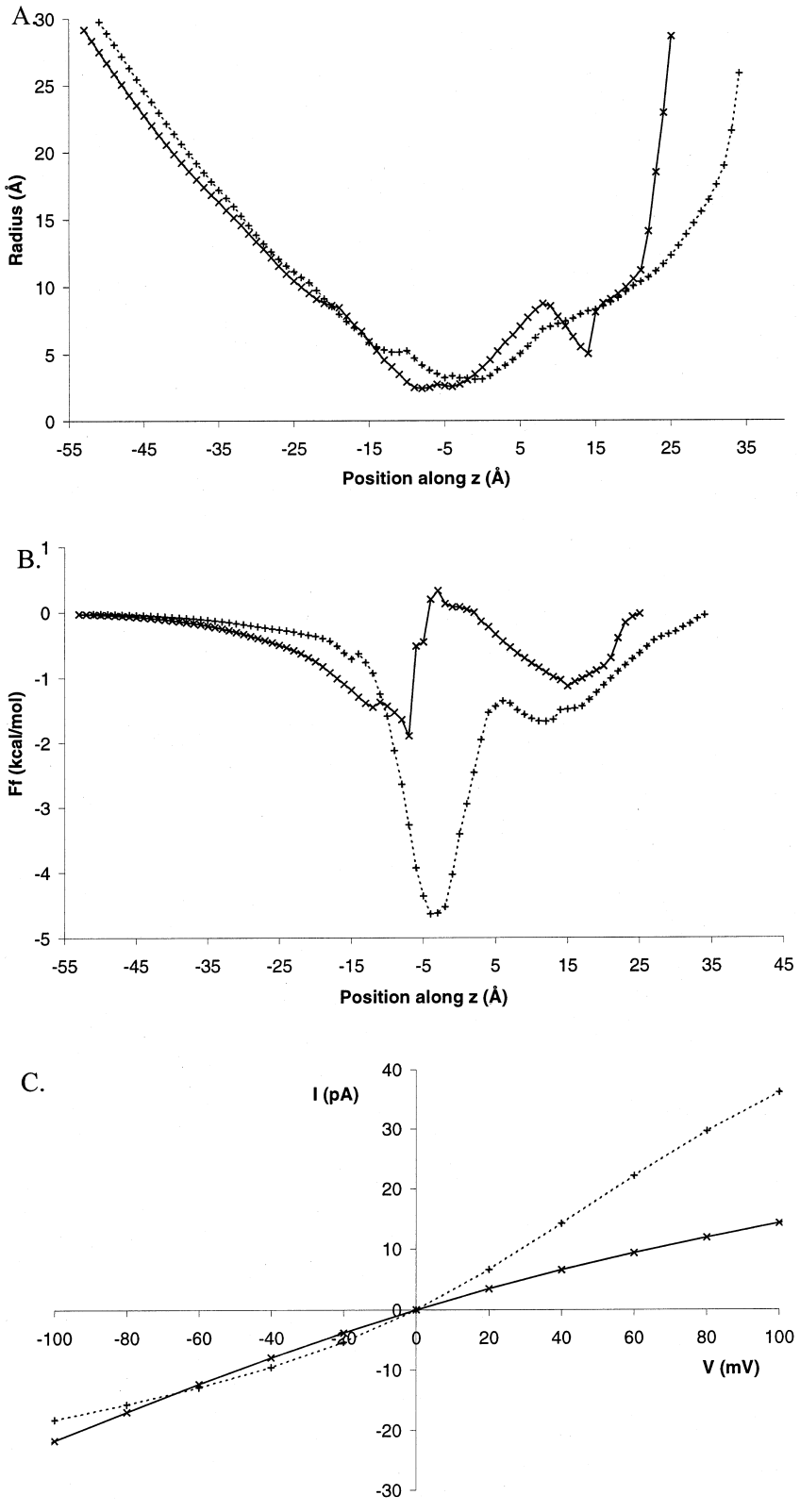

Fig. 4A–C. Results for LamB and ScrY. *Solid line* = LamB; *broken line* = ScrY. **A** Pore radius versus position along pore axis. **B** Electrostatic potential energy profile for a cation passing down the pore versus position along the pore axis. **C** *I–V* relation, at an ionic concentration of 1 M KCl

ference in channel conductance, despite pronounced structural similarities, provides us with a valuable test of theoretical treatments of single-channel conductances.

Pore radius profiles of the two glycoporin monomers (see Fig. 4A) reveals little difference between the pore geometries other than a slightly wider external (extracellular) mouth for ScrY. Conductance calculations based on these profiles yield a conductance ratio of 1.3:1 (ScrY:LamB) compared to the 10:1 determined experimentally. Thus, the difference in conductance between LamB and ScrY does not appear to be due to differences in the geometry of the channels.

Electrostatic potential profiles (see Fig. 4B) are markedly different for the two glycoporins. The LamB profile is flatter with wells at −10 Å and 15 Å of magnitude between −1 and −2 kcal/mol and a slight barrier (ca. +0.5 kcal/mol) close to the middle of the pore. In contrast, the ScrY profile shows a much deeper well (ca. −5 kcal/mol) near the middle of the pore. Thus, although both pores would be anticipated to be somewhat cation selective, different single channel conductances and *I–V* relations are anticipated.

The *I–V* relations (see Fig. 4C) derived from the electrostatic profiles are different for the two channels. In the positive quadrant the ScrY conductance (ca. 0.35 nS in 1 M KCl) is markedly greater than that of LamB (ca. 0.1 nS in 1 M KCl), whilst at negative potentials the two channels have about the same conductance. Whilst these calculations are preliminary, having not yet taken into account the absolute pK_A values of the pore-lining sidechains, they do suggest that differences in electrostatic potential energy profiles, rather than pore geometry, underlie the large differences in conductance of LamB and ScrY.

4 Discussion

We have presented applications of two methods for calculating single-channel conductances. They work at different levels. The geometry-based conductance prediction assumes that solvent and ions within a channel behave as in bulk solution. Many MD studies [24–27] of channels, including an earlier model of the H5 region of the potassium channel [8], show that water within a channel exhibits restricted motion. More recently, this has also been observed for ions within channels [28]. Moreover, pore water aligns itself to local *E*-fields and shows some ordering and hydrogen-bonding. These effects will reduce the dielectric constant within a pore and alter the resistivity [29]. The use of an empirical scale factor in the prediction of conduction at the moment provides only a first-order approximation to such considerations.

The electrostatic-based conductance prediction works at a mesoscopic level. It relies on a picture of the electrostatic field within a pore that emerges from Poisson-Boltzmann calculations and so suffers from such sources of error as all such calculations on proteins. The determination of the sidechain ionisation state is dependent on the exact sidechain conformations within a structure, as revealed by calculations of successive snapshots from a MD simulation show differing pictures. In calculating an electrostatic potential along the axis of a pore and the resultant *I–V* curves we are reducing the problem to a one-dimensional approximation. The *I–V* calculation utilises bulk values for the diffusion constant of ions. However, despite such approximations, the results presented here are encouraging, correctly predicting cation selectivity and approximate conductances.

The work on the model potassium channel clearly shows the need to consider the ionisation state of titratable groups. These have marked effects on channel function. This suggests that the ionisation state of such sidechains deserve consideration when probing the structure-function relation on the basis of experimental X-ray structures of channels. The glycoporin analyses highlight the importance of electrostatic calculations in addressing experimentally observed differences in conductance where geometric considerations alone are insufficient.

Acknowledgements. We are grateful to Prof. Wolfram Welte for kindly providing us with the coordinates for ScrY. This work is supported by grants from The Wellcome Trust.

References

1. Hille B (1992) Ionic channels of excitable membranes, 2nd edn. Sinauer, Sunderland, Mass
2. Colquhoun D, Sigworth FJ, Neher E (1983) Fitting and statistical analysis of single-channel records. Plenum, New York
3. Doyle DA, Cabral JM, Pfuetzner RA, Kuo A, Gulbis JM, Cohen SL, Chait BT, Mackinnon R (1998) Science 280:69
4. Barcilon V, Chien D-P, Eisenberg RS (1992) SIAM J Appl Math 52:1405
5. Smart OS, Breed J, Smith GR, Sansom MSP (1997) Biophys J 72:1109
6. Sankararamakrishnan R, Adcock C, Sansom MSP (1996) Biophys J 71:1659
7. Karshikoff A, Spassov V, Cowan SW, Landenstein RAST (1994) J Mol Biol 240:372
8. Ranatunga KM, Kerr ID, Adcock C, Smith GR, Sansom MSP (1998) Biochim Biophys Acta 1370:1
9. Schirmer T, Kellar TA, Wang YF, Rosenbusch JP (1995) Science 267:512
10. Forst D, Welte W, Wacker T, Diedrichs K (1998) Nat Struct Biol 5:37
11. Smart OS, Goodfellow JM, Wallace BA (1993) Biophys J 65:2455
12. Davis ME, Madura JD, Luty BA, McCammon JA (1991) Comput Phys Commun 62:187
13. Bashford D, Gerwert K (1992) J Mol Biol 224:473
14. Adcock C, Smith GR, Sansom MSP (1998) Biophys J 75:1211–1222
15. Kerr ID, Sansom MSP (1997) Biophys J 73:581
16. Heginbotham L, MacKinnon R (1993) Biophys J 65:2089
17. Weiss MS, Kreusch A, Schiltz E, Nestel U, Welte W, Weckesser J, Schulz GE (1991) FEBS Lett 280:379
18. Cowan SW, Schirmer T, Rummel G, Steiert M, Ghosh R, Apuptit RA, Jansonius JN, Rosenbusch JP (1992) Nature 358:727
19. Kreusch A, Neubueser A, Schiltz W, Wekesser J, Schulz GE (1994) Protein Sci 3:58
20. Hirsch A, Wacker T, Weckesser J, Diederichs K, Wolfram W (1995) Proteins: Struct Funct Genet 23:282
21. Benz R, Schmid A, Nakae T, Vos-scheperkeuter GH (1986) J Bacteriol 165:978
22. Schluein K, Benz R (1990) Mol Microbiol 4:625
23. Schluein K, Schmid K, Benzl R (1991) Mol Microbiol 5:2233
24. Breed J, Sankararamakrishnan R, Kerr ID, Sansom MSP (1996) Biophys J 70:1643
25. Sansom MSP, Kerr ID, Breed J, Sankararamakrishnan R (1996) Biophys J 70:693
26. Sansom MSP, Breed J, Sankararamakrishnan R, Kerr ID (1996) Biochem Soc Trans 24:S139
27. Sansom MSP, Kerr ID, Biggin PC, Mitton PA (1996) Biophys J 70:A231
28. Smith GR, Sansom MSP (1998) Biophys J 75:(in press)
29. Sansom MSP, Smith GR, Adcock C, Biggin PC (1997) Biophys J 73:2404